HHS Public Access

Author manuscript

IEEE Int Conf Robot Autom. Author manuscript; available in PMC 2020 May 04.

Published in final edited form as:

IEEE Int Conf Robot Autom. 2019 May ; 2019: 9073–9079. doi:10.1109/ICRA.2019.8793658.

Adaptive Control of Sclera Force and Insertion Depth for Safe Robot-Assisted Retinal Surgery

Ali Ebrahimi, **Niravkumar Patel [Member, IEEE]**

Department of Mechanical Engineering and Laboratory for Computational Sensing and Robotics at the Johns Hopkins University, Baltimore, MD 21218 USA

Changyan He,

Department of Mechanical Engineering and Laboratory for Computational Sensing and Robotics at the Johns Hopkins University, Baltimore, MD 21218 USA

School of Mechanical Engineering and Automation at Beihang University, Beijing, 100191 China

Peter Gehlbach [Member, IEEE]

Wilmer Eye Institute, Johns Hopkins Hospital, Baltimore, MD 21287 USA

Marin Kobilarov, **Iulian Iordachita [Senior Member, IEEE]**

Department of Mechanical Engineering and Laboratory for Computational Sensing and Robotics at the Johns Hopkins University, Baltimore, MD 21218 USA

Abstract

One of the significant challenges of moving from manual to robot-assisted retinal surgery is the loss of perception of forces applied to the sclera (sclera forces) by the surgical tools. This damping of force feedback is primarily due to the stiffness and inertia of the robot. The diminished perception of tool-to-eye interactions might put the eye tissue at high risk of injury due to excessive sclera forces or extreme insertion of the tool into the eye. In the present study therefore a 1-dimensional adaptive control method is customized for 3-dimensional control of sclera force components and tool insertion depth and then implemented on the velocity-controlled Johns Hopkins Steady-Hand Eye Robot. The control method enables the robot to perform autonomous motions to make the sclera force and/or insertion depth of the tool tip to follow pre-defined desired and safe trajectories when they exceed safe bounds. A robotic light pipe holding application in retinal surgery is also investigated using the adaptive control method. The implementation results indicate that the adaptive control is able to achieve the imposed safety margins and prevent sclera forces and insertion depth from exceeding safe boundaries.

I. INTRODUCTION

Vitreoretinal surgery is among the most delicate surgical tasks in which physiological hand tremor may severely attenuate surgeon performance and put the eye at high risk of injury. Robot-assisted retinal surgery is potentially beneficial as it enhances tool tip position accuracy and suppresses involuntary hand-tremor. Robots developed for eye-surgery can be

aebrahi5@jhu.edu.

classified as collaborative or tele-operated. An example of collaborative robotic systems in which surgeon and robot share control of the surgical tool, is the Steady-Hand Eye Robot (SHER) developed here at the Johns Hopkins University [1], [2] (Fig. 1-a). Another 4-DoF (degrees of freedom) collaborative robotic arm for manipulation in highly confined spaces around an incision point was designed and fabricated by Gijbels et al. [3]. Wei et al. have also presented a hybrid two-armed robotic system for dexterity enhancement in intraocular maneuvers [4]. Using a parallel coupled joint mechanism, Nasseri et al. designed and developed a compact robotic system for intraocular manipulation [5].

In terms of tele-operated microsurgical systems, Ikuta et al. proposed a 5-DoF slave micro manipulator [6]. Using spherical guides architecture for the slave manipulator, the University of Tokyo designed and fabricated a tele-operated system having 40 to 1 scale down from master motion to slave maneuvers [7], [8]. In a very recent study, Wilson et al. built a master-slave robotic system called IRISS with a laser based control of the remote center of motion (RCM) point [9]. The most clinically advanced robotic assistance in eye surgery is described in the recent studies of Edwards et al. [10] and Gijbels et al. [11] with which they conducted first in-human robot-assisted eye surgeries. As an alternative to the table-mounted robotic systems, Riviere et al. developed an active tremor canceling device, Micron [12]. Moreover, an electromagnetic system called OctoMag was developed by Kummer et al. to control intraocular microrobots to perform delicate surgical tasks [13].

Integrating robots into eye surgery has produced safety challenges. The stiffness and inertia of the robot that is between the surgeon and the surgical target may diminish the surgeon’s perception and control over scleral forces, tool tip forces and insertion depth (Fig. 1-b). This in turn leads to larger sclera forces during robot-assisted eye surgery [14], [15]. There is now prior work attempting to restore this sensory information to surgeons in order to enhance safety. Cutler et al. have used auditory feedback to limit tool tip forces from exceeding safe boundaries during membrane peeling [16]. Ebrahimi et al. have reported protection of sclera tissue when auditory or haptic feedback is provided based on sclera force [17].

Auditory substitution or haptic feedback that has been deployed in the previous studies may have some disadvantages. First, the efficacy of feedback is highly dependent on the surgeon’s reaction to it. In cases where effective action was barely executable by the subjects or when unexpected eye motion occurred, scleral forces could increase beyond safe limits [17]. Furthermore, it is now feasible to build in similar haptic and audio feedback based on tool insertion depth to enhance tool depth safety (if exceeded tool tip to retina collision occurs). However, having various types of audio and haptic feedback coming from different sources may have adverse effects on surgeon concentration during highly delicate, prolonged and intensely focused eye surgery tasks. For these and other reasons, it is potentially beneficial to control the robot such that it acts autonomously in a proper and safe way when sclera force or tool insertion depths exceed established safe boundaries. To fulfill these purposes in this study, a 1-D adaptive control method is customized for simultaneous 3-D control of sclera force and insertion depth. When the adaptive control is triggered, the robot produces translational motions along the relevant axes to correct the sclera force and/or insertion depth consistent with desired and safe trajectories. This control system is then implemented on the SHER (Fig. 1-a). The adaptive control method has other useful

applications in eye surgery including: control of the insertion depth when unexpected motion of the patient's head is observed or holding a light pipe in a fixed and safe position by the robot. To the best of our knowledge, adaptive control for applications in robot-assisted eye surgery has not been used before.

In section II, concept of the 1-D adaptive control is explained. In section III, the impedance control of the SHER is elaborated. Then the way the 1-D adaptive control is customized for 3-D control of sclera force and insertion depth is described and possible applications in eye surgery are discussed. In section IV, after illustrating the experimental setup the adaptive force and insertion depth controls are implemented on the SHER to obtain safety enhancing applications in retinal surgery and the results are provided. The results are discussed in section V.

II. REVIEW OF ADAPTIVE CONTROL

Our control strategy builds upon the adaptive force control method developed by [18] for general 1-DoF robots and extends it to the eye surgery domain. There are two basic assumptions for this method:

1. The robot is in contact with an environment with unknown but linear stiffness/compliance (Fig. 2). In other words, the force displacement model of the robot end-effector is assumed to conform to the linear equation of $f_e = \frac{1}{\gamma}(x - x_0)$ or $df_e = \frac{1}{\gamma}(dx)$ where f_e is the interaction force exerted to the robot by the flexible environment, γ is a constant representing the environment compliance, x is the position of the 1-DoF robot and x_0 is the equilibrium point.
2. The robot is a velocity-controlled robot, i.e. it has a built-in low-level velocity controller that makes the robot's actual velocity $\dot{x}$ track any bounded velocity setpoint $\dot{x}_d$.

The goal of the 1-D adaptive control is to design a control law which provides asymptotically exact outer loop force control by providing proper reference velocity trajectory ($\dot{x}_d$) for the low-level velocity control. Consequently, the interaction force (f_e) would be able to track any desired reference force trajectory (f_d) which is C^2 bounded and has bounded derivatives, $\dot{f}_d$ and $\ddot{f}_d$. The control input and the adaptation law are provided in (1).

$$\begin{aligned} \dot{x}_d(t) &= \hat{\gamma}\dot{f}_d(t) - k_f\Delta f(t) \\ \dot{\hat{\gamma}} &= -\alpha\dot{f}_d(t)\Delta f(t) \end{aligned} \tag{1}$$

where the term $\Delta f \triangleq f_e - f_d$ is the force tracking error. The constants α and k_f are gains for adaptation law and the force tracking error, respectively. Since it was assumed that the compliance of the environment is unknown, an estimation of this parameter ($\hat{\gamma}$) is used in the control law above. The adaptation law defines the way $\hat{\gamma}$ changes over time. Using a Lyapunov function it is proved that the force tracking error Δf and the compliance estimation

$\hat{\gamma}$ will remain bounded. Moreover, one can show that $\lim_{t\to\infty} \Delta f(t) = 0$ if the conditions given in (2) are satisfied [18].

$$\int \left|\Delta \dot{x}\right|^2 dx < \infty \quad and \quad \lim_{t \to \infty} \Delta \dot{x} = 0 \tag{2}$$

In (2), the term $\Delta \dot{x}$ is the velocity tracking error $\dot{x} - \dot{x}_d$ and based on the second assumption discussed earlier, it would converge to zero. Thus, based on (2) the adaptive control will make Δf go to zero.

III. RETINAL ADAPTIVE CONTROL METHOD

The purpose of this study is to customize the adaptive control strategy mentioned in section II for 3-D applications in robot-assisted retinal surgery to improve safety. The application developed in this study include sclera force adaptive control, insertion depth adaptive control and robot-assisted light pipe control. Prior to explaining the methods, it is important to understand the SHER and its general impedance control law.

SHER is a cooperatively velocity-controlled (assumption 2 in section II is satisfied) 5-DoF robot (including three translational motions for the entire robot and two rotational roll and pitch motions for the end-effector) developed at the Johns Hopkins University (Fig. 1-a). Different eye surgical tools can be attached to the robot end-effector. The mechanical design of the robot takes advantage of a fixed RCM point which makes the surgical tool pass through that point when the translational degrees of freedom of the robot are fixed. Two coordinate frames are considered for the robot: 1) B, the body coordinate frame which is attached to the RCM point and is rigid to the end-effector and the surgical tool. As it is apparent from Fig. 1-a, the surgical tool is always directed toward the z direction of the body frame. 2) A, the spatial coordinate frame which is fixed and located at the robot base (shown in Fig. 1-a).

The robot acts as a cooperative assistant to the surgeon in the following way; the surgeon holds the tool handle while it is attached to the robot and moves it with the assistance of the robot to insert the surgical tool into the eye and perform surgical tasks. The interaction force applied to the tool handle by the surgeon ($f_h \in \mathbb{R}^6$ whose point of application is represented in Fig. 1-a) is measured in the body coordinate frame by a force/torque sensor placed under the RCM mechanism as shown in Fig. 1-a and is denoted by f_h^b. The superscript b indicates that the vector is represented in the body frame.

The forces f_{sx}, f_{sy}, are x and y components of sclera force in the body frame. The z component of the sclera force is supposed to be zero because of the negligible friction between the tool shaft and eyeball. Insertion depth is the length of the tool inserted into the eyeball (Fig. 1-b).

The forward kinematics of the robot and the robot jacobian are as following:

$$X^s = f(q)$$
$$\dot{X}^s = \boldsymbol{J}(q)\dot{q} \tag{3}$$

where $q \in \mathbb{R}^5$ is the vector of robot joint angles and $X^s \in \mathbb{R}^6$ is the vector which defines the position and orientation of the body frame with respect to the spatial coordinate frame. The first three elements of X^s are the position of the RCM point expressed in the spatial frame, and the last three elements of X^s are the Euler angles of the body frame with respect to the spatial frame. The second equation in (3) is obtained by deriving the first one with respect to time. Therefore, $X^s \in \mathbb{R}^6$ is the translational and angular velocities of the body frame represented in the spatial frame ($\dot{X}^b$ is the same vector represented in the body frame). Vector $\dot{q} \in \mathbb{R}^5$ is the robot joint velocities and $J(q)$ denotes the robot jacobian matrix. The normal impedance control of the robot (before applying any adaptive control which is the purpose of this paper) would be as following:

$$\dot{X}_d^b = \Gamma f_h^b \tag{4}$$

where $\dot{X}_d^b$ is the desired velocity of the end-effector expressed in the body frame. The matrix $\Gamma \in \mathbb{R}^{6x6}$ is a constant diagonal matrix with positive elements. This controller sets a desired velocity for the end-effector proportional to the force applied by the surgeon to the tool handle which causes the robot to move in a collaborative way with the surgeon. Having the forward kinematics of the robot, the vector $\dot{X}_d^b$ is transferred to the spatial frame to get $\dot{X}_d^s$. Then, using the pseudo inverse of the robot jacobian , $J^{\dagger}(q)$, the desired joint velocities are calculated.

$$\dot{q}_d = \boldsymbol{J}^{\dagger}(q)\dot{X}_d^s \tag{5}$$

The vector $\dot{q}_d$ is then passed to the low-level joint velocity controller of the SHER.

A. Scleral force control

The first assumption for the adaptive control in section II states that the environmental force f_e should be linearly proportional to the position of the robot in the coordinate frame where $\dot{x}_d(t)$ is going to be calculated (df_e should be proportional to dx). Now assume that at each instant of robot motion we have a fixed frame B' coincident with B. We assume that the infinitesimal variation of the sclera force in x and y directions of body frame, df_{sx} and df_{sy}, are linearly proportional to the infinitesimal variation of the position of the RCM point along the x and y directions of B', dx_{rcm} and dy_{rcm}. This assumption is realized because the tool shaft is like a cantilever beam, and therefore the infinitesimal variation of the force applied to the beam (which is now df_{sx} or df_{sy}) is proportional to the infinitesimal variation of the beam deflection (which is now dx_{rcm} and dy_{rcm}). Therefore. we can make use of the adaptive control law to produce desired velocities for the robot end-effector along the x or y axes of the body frame ($\dot{x}_d^b(t)$ or $\dot{y}_d^b(t)$) such that f_{sx} and f_{sy} will follow desired and

presumably safe trajectories. Compared to (1), we are using either f_{sx} or f_{sy} to substitute f_e. In (6), the adaptive sclera force control for f_{sx} is provided and explained in the following. For the y direction similar equations and procedure can be imagined.

$$\begin{aligned} \dot{x}_d^b(t) &= \hat{\gamma}_x \dot{f}_{dx}(t) - k_{fx}\Delta f_x(t), \\ \dot{\hat{\gamma}}_x &= -\alpha_x \dot{f}_{dx}(t)\Delta f_x(t), \end{aligned} \tag{6}$$

In (6), $\Delta f_x = f_{sx} - f_{dx}$ is the sclera force tracking error. The term $f_{dx}(t)$ denotes the desired trajectory for f_{sx} and $\dot{f}_{dx}(t)$ is the derivative of f_{sx}. Note that $\dot{x}_d^b(t)$ and $\dot{y}_d^b(t)$ will be the first and second elements of the vector $\dot{X}_d^b$ and other elements of $\dot{X}_d^b$ will be still generated using f_h^b according to (4). In other words, the robot will abide by the user's interaction forces for other elements of $\dot{X}_d^b$. Thus, the users would not feel that the robot inhibits their manipulation.

After constructing $\dot{X}_d^b$, $\dot{X}_d^s$ can be obtained using the forward kinematics of the robot. Using (5), the term $\dot{q}_d$ can eventually be found. Thus, by this adaptive sclera force control we can make the SHER to move in such a way to make the x and y components of sclera force to follow desired trajectories laying in safe ranges. This control can be independently triggered for f_{sx} or f_{sy} whenever any of these components exceed safe levels to reduce them on desired declining trajectories.

B. Tool insertion depth control

In this application we will customize the adaptive control algorithm to control the insertion depth of the surgical tool by replacing the term f_e in (1) with the insertion depth D. In other words, any variable whose infinitesimal variation satisfies the first assumption in section II can be used instead of f_e. Following the same explanation provided in section III-A, at each instant the infinitesimal variation of insertion depth D is proportional to the infinitesimal variation of the RCM point position along the z axis of the frame B'. Thus, we can produce desired velocities for the end-effector along the z axis of the body frame such that now the insertion depth will track a desired and safe reference trajectory. The control can be triggered whenever the insertion depth exceeds certain limits which may lead to collision between the tool tip and the retina. The control law and the adaptation law for the insertion depth control are provided in (7):

$$\begin{aligned} \dot{z}_d^b(t) &= \hat{\gamma}_z \dot{D}_d(t) - k_{fz}\Delta D(t), \\ \dot{\hat{\gamma}}_z &= -\alpha_z \dot{D}_d(t)\Delta D(t), \end{aligned} \tag{7}$$

where $\Delta D = D(t) - D_d(t)$ is the insertion depth tracking error. The term D_d denotes the desired trajectory for D and $\dot{D}_d$ is the derivative of D_d. Note that $D_d(t)$ will be the third element of the vector $\dot{X}_d^b$. In fact, at any necessary time any of the first three elements of the can be switched to the adaptive control method while other elements continue to be generated based on the general impedance control (4).

After calculating $\dot{X}_d^b$, the same procedure explained in section III-A should be followed to find the $\dot{q}_d$.

IV. EXPERIMENTAL SETUP AND RESULTS

To prove the applications of the adaptive control on the SHER, we prepared the experimental setup depicted in Fig. 3. The user's force applied to the handle f_h^b is measured by the 6-DoF ATI force/torque sensor which is attached under the robot wrist (Fig. 3-a). The user should hold the tool handle and insert it through the sclerotomy point (Fig. 3-b) to manipulate the eyeball.

To simultaneously measure f_{sx} and f_{sy} and insertion depth which are the basis of the adaptive controllers developed, we built a dual force-sensing tool by attaching three Fiber Bragg Grating (FBG) strain sensors with outer diameter of $80\mu m$ around the perimeter of the surgical tool. Then the tool was calibrated following the instructions given by [19]. The root mean square error for the sclera force and insertion depth measurements were calculated and are 3.8 mN and 0.29 mm, respectively. The FBG fibers are connected to an optical sensing interrogator (sm130–700 from Micron Optics Inc., Atlanta, GA). The interrogator then sends the FBG raw data to computer using a TCP/IP connection, and then the relevant calibration matrices will be applied to calculate real-time values of the sclera force components and insertion depth. Next, based on the relevant control laws (adaptive or impedance) each component of the vector $\dot{X}_d^b$ is computed. Finally, $\dot{q}_d$ will be sent to the low-level embedded robot controller (Galil 4088, Galil, 270 Technology Way, Rocklin, CA 95765) which is the motor driver (low-level velocity controller of the SHER). The loop frequency for the system is 1 KHz and the data is recorded with frequency of 200 Hz. All of the data transmission, collection and manipulation were performed through the software package (developed using the CISST framework, a collection of libraries for development of computer-assisted intervention systems; InfinityQS, Fairfax [16]).

To model simple surgical tasks in eye surgery, we placed an artificial eye phantom made from Silicon into a 3D-printed socket. To produce a realistic eye ball motion, the interface between the eye phantom and the eye socket was lubricated with mineral oil. Moreover, painted vessels were attached inside the eye ball on the posterior part, Fig. 3-b.

In the following, the implementations of the adaptive control for the three applications of sclera force control, insertion depth control and the robot-assisted light pipe holding are explained and the results are represented.

A. Sclera force safety

First, to show the performance and functionality of the adaptive force control that the controller can actually follow the desired trajectories for f_{sx} and f_{sy}, a sinus wave of 40 $\sin(2t)$ mN and $-40\sin(2t)$ mN were set for the f_{dx} and f_{dy}, respectively. Thus, the first two elements of $\dot{X}_d^b$ were produced based on the adaptive control and the remaining four elements of $\dot{X}_d^b$ were set to zero. The results for this implementation are shown in Fig. 4. The

root mean squared error for f_{sx} and f_{sy} tracking errors for the interval of $0 < t < 20$ in Fig. 4, were calculated to be 7.31 and 9.44 mN, respectively.

Secondly, the adaptive force control is utilized to maintain the sclera force within the safe bounds. Based on the data recorded from the behavior of an expert surgeon, an upper bound of 120 mN for sclera force was assigned as the safe limit [17]. In this study, we have kept this value as the upper bound for f_{sx} and f_{sy}. Whenever f_{sx} exceeds 100 mN the adaptive control for f_{sx} is triggered and the desired trajectory in (8), which is an exponentially decreasing path, is set for the sclera force (for the y component of sclera force a similar desired path can be imagined). If f_{sx} exceeds −100 mN, a negative sign should be applied to the right-hand side of (8). The reason for choosing 100 here is to trigger the controller in advance, in order to hinder the sclera forces to reach the upper limits of safety here being 120 mN.

$$f_{dx}(t) = a_f\left(e^{-b_f(t - t_{0x})} + 1\right), \tag{8}$$

where a_f is a constant (in our experiments setting $a_f = 55$ made reasonable robot behaviour). The parameter b_f indicates how fast the sclera force is declined. After trying various quantities for b_f, it was set to one because for this value the robot showed a reasonable trade-off between speed and smoothness.

Thus, the robot will move such that f_{sx} will follow the declining path specified in (8). In (8), t_{0x} is the time when f_{sx} exceeds 100 mN after which the adaptive control is triggered. At time $t = t_{0x}$, f_{dx} in (8) equals 110 mN which is close to f_{sx} at $t = t_{0x}$ which is 100 mN to have a continues and smooth motion when switching to adaptive mode. The robot is switched back to the collaborative mode (equation (4)) for x direction after f_{sx} is brought down to 70 mN. The adaptive control will be activated again if f_{sx} exceeds 100.

Thus, the first element of $\dot{X}_d^b$ (in case of f_{sy} it would be the second element of $\dot{X}_d^b$) is generated based on (6) while having (8) as the f_{dx}. As mentioned earlier, other elements of $\dot{X}_d^b$ would still be generated based on f_h^b. This will actually cause the robot to act as a safety assistant along the x or y axes of the body frame until the sclera force is brought back to safe levels, and thus the surgeon does not feel that the robot is disrupting his/her maneuver.

After setting up the adaptive force control for sclera safety, using the experimental setup the task of following two painted vessels on retina (the blue and the orange vessels in Fig. 3-b) was performed and the data was recorded. A user followed these two vessels from the home position to the end with the tool tip without touching the vessels. The results for f_{sx} and f_{sy} are shown in Fig. 5. For this experiment the values of k_{fx} and k_{fy} were both set to 0.2 and the values of α_x and α_y were both set to 0.00005 (for (6)).

B. Insertion depth safety

A scenario similar to the sclera force safety has been set for the insertion depth safety. Because the diameter of the eye phantom is around 25 mm a threshold of 20 has been set after which the adaptive control for the z direction of the body frame will be activated to

retract the tool and bring down the insertion depth on a desired exponential declining path. Thus, the robot does not allow the insertion depth to exceed 20 mm. The following desired trajectory is set for the insertion depth.

$$D_d(t) = a_D\left(e^{-b_D(t - t_{0z})} + 1\right) \tag{9}$$

where t_{0z} is the time when the insertion depth exceeds 20 mm after which the adaptive control is triggered. The terms a_D and b_D are constants and are set to 10 and 2, respectively. The reason for choosing this values is the same as what was explained in section IV-A. At the time $t = t_{0z}$, D_d in (9) equals 20 mm which is the same as the value of insertion depth at $t = t_{0z}$ which is 20 mm to have a continues and smooth motion when switching to adaptive mode in z direction. For this part the same vessel following task described in IV-A (just one of the vessels) was done to evaluate the performance of the insertion depth control. The variation of insertion depth for this part is depicted in Fig.6. For this experiment the values of k_{fz} and α_z were set to 10 and 0.0005, respectively (for (7)).

C. Robot-assisted light pipe holding

In this application the robot holds the light pipe inside the eye and moves it in a safe way commensurate with the surgeon's manipulation of the eyeball. There may be two safety concerns for this application. While the surgeon is manipulating the eyeball with another surgical tool, it may cause the light pipe which is held by the robot to exert excessive forces to the sclera or to allow the light pipe tip to make contact with retina if the insertion depth goes beyond a safe level. The methods discussed in sections III-A and III-B if applied simultaneously are able to address these safety issues together to achieve a safe light pipe holding application.

Here, f_{dx} and f_{dy} are set to constant values $60mN$ and $-60mN$, respectively. By assigning a constant value for the desired sclera force the robot will move accordingly and smoothly while the surgeon is rotating the eyeball with another surgical tool. Therefore, the light pipe shaft will always apply the same safe force to the sclera and sclera tissue safety is guaranteed. The adaptive insertion depth control is also kept activated based on (9). Thus, if the tip of the light pipe gets too close to the retina while the surgeon is rotating the eyeball, the robot will retract the light pipe along the light pipe axis (z axis of the body frame) to avoid collision between the light pipe tip and the retina which is considered a serious complication. It is important to note that in robot-assisted light pipe holding the adaptive sclera force and insertion depth controls are always kept activated and will not be switched back to the collaborative impedance control.

To demonstrate this function, the force-sensing tool is used as a light pipe and is kept in the eye by the robot while the eyeball is rotated by another instrument. The plots for sclera force and insertion depth for this part are shown in Fig. 7.

V. DISCUSSION AND CONCLUSION

Fig. 4 demonstrates that using the adaptive control the robot is able to follow the desired sinusoidal force for f_{sx} and f_{sy} with comparatively small amplitude of 40 mN with good

accuracy. In the last part of Fig. 4 (from time $t = 23s$ to $t = 25s$), the desired trajectories are not followed because the adaptive control is stopped after $t = 23s$. Based on Figs. 5 and 6, it is observed that the robot is acting properly to bring down the sclera force components or the insertion depth through their desired exponential trajectories which are shown with interrupted discontinuous lines with short lengths (the period when the adaptive control is activated) in each figure. The reason for such short lengths is that using the adaptive controls the SHER requires only a very small autonomous motion (up to 2 mm) to return the sclera forces or insertion depth to safe limits. Therefore, the period of time the adaptive controls are active would be short.

The reason for choosing an exponential desired trajectory is that it has steep slope at the moment of safety violation for sclera force or insertion depth, so the robot will act fast enough at the start of the incident to prevent any harm. Moreover, the exponential function drops fast enough to reach to the safe levels.

It is important to note that in the provided figures the real sclera force or the insertion depth may deviate slightly from their desired trajectories. The reason is that as mentioned before, when the robot is switched to adaptive control, the relevant values in $\dot{X}_d^b$ are computed based on the adaptive controller and all the other entities of $\dot{X}_d^b$ are still calculated based on (4). Thus, for example, for the rotational movements (last three elements of $\dot{X}_d^b$) the robot is always obeying the user's force, f_h^b. This rotational motion of the robot would affect the control variables most notably the scleral force causing a deviation from the desired trajectories. However, the adaptive controller tries to account for this and as it is observed the control variables continue to follow their desired trajectories with an acceptable accuracy.

Current limitation of our work is that the tool must be kept fixed relative to the robot end-effector and cannot rotate around its axis, so the tool coordinate frame would be always aligned with the body frame. Thus, we will have the measured sclera forces in the body frame as required for the adaptive control. In the future, by attaching a rotary encoder to the tool it would be possible to implement the same adaptive control strategy while the tool is free to rotate.

To sum up, in this paper we explored the feasibility of extending a 1-D adaptive control for 3-D applications in robot-assisted eye surgery including the sclera force control, insertion depth control and the robot-assisted light pipe holding. Several experiments were then conducted to evaluate how these three applications may contribute to safe robot-assisted retinal surgery. In the future we plan to expand the range of tasks, conduct multi-user experiments to evaluate the control performance under different behaviors, and also transition to in-vivo experiments.

Acknowledgments

This work was supported by U.S. National Institute of Health under grant number of 1R01EB023943-01 and Research to Prevent Blindness, New York, New York, USA, and gifts by the J. Willard and Alice S. Marriott

Foundation, the Gale Trust, Mr. Herb Ehlers, Mr. Bill Wilbur, Mr. and Mrs. Rajandre Shaw, Ms. Helen Nassif, Ms. Mary Ellen Keck, and Mr. Ronald Stiff.

REFERENCES

[1]. Taylor R, Jensen P, Whitcomb L, Barnes A, Kumar R, Stoianovici D, Gupta P, Wang Z, Dejuan E, and Kavoussi L, "A steady-hand robotic system for microsurgical augmentation," The International Journal of Robotics Research, vol. 18, no. 12, pp. 1201–1210, 1999.

[2]. Fleming I, Balicki M, Koo J, Iordachita I, Mitchell B, Handa J, Hager G, and Taylor R, "Cooperative robot assistant for retinal microsurgery," in International conference on medical image computing and computer-assisted intervention. Springer, 2008, pp. 543–550.

[3]. Gijbels A, Wouters N, Stalmans P, Van Brussel H, Reynaerts D, and Vander Poorten E, "Design and realisation of a novel robotic manipulator for retinal surgery," in Intelligent Robots and Systems (IROS), 2013 IEEE/RSJ International Conference on. IEEE, 2013, pp. 3598–3603.

[4]. Wei W, Goldman R, Simaan N, Fine H, and Chang S, "Design and theoretical evaluation of micro-surgical manipulators for orbital manipulation and intraocular dexterity," in Robotics and Automation, 2007 IEEE International Conference on. IEEE, 2007, pp. 3389–3395.

[5]. Nasseri MA, Eder M, Nair S, Dean E, Maier M, Zapp D, Lohmann CP, and Knoll A, "The introduction of a new robot for assistance in ophthalmic surgery," in 2013 35th Annual International Conference of the IEEE Engineering in Medicine and Biology Society (EMBC). IEEE, 2013, pp. 5682–5685.

[6]. Ikuta K, Yamamoto K, and Sasaki K, "Development of remote microsurgery robot and new surgical procedure for deep and narrow space," in Robotics and Automation, 2003. Proceedings. ICRA'03. IEEE International Conference on, vol. 1 IEEE, 2003, pp. 1103–1108.

[7]. Ueta T, Yamaguchi Y, Shirakawa Y, Nakano T, Ideta R, Noda Y, Morita A, Mochizuki R, Sugita N, Mitsuishi M et al., "Robot-assisted vitreoretinal surgery: Development of a prototype and feasibility studies in an animal model," Ophthalmology, vol. 116, no. 8, pp. 1538–1543, 2009. [PubMed: 19545902]

[8]. Noda Y, Ida Y, Tanaka S, Toyama T, Roggia MF, Tamaki Y, Sugita N, Mitsuishi M, and Ueta T, "Impact of robotic assistance on precision of vitreoretinal surgical procedures," PloS one, vol. 8, no. 1,p. e54116, 2013. [PubMed: 23335991]

[9]. Wilson JT, Gerber MJ, Prince SW, Chen C-W, Schwartz SD, Hubschman J-P, and Tsao T-C, "Intraocular robotic interventional surgical system (iriss): Mechanical design, evaluation, and master–slave manipulation," The International Journal of Medical Robotics and Computer Assisted Surgery, vol. 14, no. 1, p. e1842, 2018.

[10]. Edwards T, Xue K, Meenink H, Beelen M, Naus G, Simunovic M, Latasiewicz M, Farmery A, de Smet M, and MacLaren R, "First-in-human study of the safety and viability of intraocular robotic surgery," Nature Biomedical Engineering, p. 1, 2018.

[11]. Gijbels A, Smits J, Schoevaerdts L, Willekens K, Vander Poorten EB, Stalmans P, and Reynaerts D, "In-human robot-assisted retinal vein cannulation, a world first," Annals of Biomedical Engineering, pp. 1–10, 2018.

[12]. MacLachlan RA, Becker BC, Tabarés JC, Podnar GW, Lobes LA Jr, and Riviere CN, "Micron: an actively stabilized handheld tool for microsurgery," IEEE transactions on robotics: a publication of the IEEE Robotics and Automation Society, vol. 28, no. 1, p. 195, 2012. [PubMed: 23028266]

[13]. Kummer MP, Abbott JJ, Kratochvil BE, Borer R, Sengul A, and Nelson BJ, "Octomag: An electromagnetic system for 5-dof wireless micromanipulation," IEEE Transactions on Robotics, vol. 26, no. 6, pp. 1006–1017, 2010.

[14]. He C, Ebrahimi A, Roizenblatt M, Patel N, Yang Y, Gehlbach PL, and Iordachita I, "User behavior evaluation in robot-assisted retinal surgery," in 2018 27th IEEE International Symposium on Robot and Human Interactive Communication (RO-MAN). IEEE, 2018, pp. 174–179.

[15]. He C, Roizenblatt M, Patel N, Ebrahimi A, Yang Y, Gehlbach PL et al., "Towards bimanual robot-assisted retinal surgery: Tool-to-sclera force evaluation," in 2018 IEEE SENSORS. IEEE, 2018, pp. 1–4.

[16]. Cutler N, Balicki M, Finkelstein M, Wang J, Gehlbach P, Mc-Gready J, Iordachita I, Taylor R, and Handa JT, "Auditory force feedback substitution improves surgical precision during simulated ophthalmic surgery," Investigative ophthalmology & visual science, vol. 54, no. 2, pp. 1316–1324, 2013. [PubMed: 23329663]

[17]. Ebrahimi A, He C, Roizenblatt M, Patel N, Sefati S, Gehlbach P, and Iordachita I, "Real-time sclera force feedback for enabling safe robot assisted vitreoretinal surgery," in 2018 40th Annual International Conference of the IEEE Engineering in Medicine and Biology Society (EMBC). IEEE, 2018, pp. 3650–3655.

[18]. Roy J and Whitcomb LL, "Adaptive force control of position/velocity controlled robots: theory and experiment," IEEE Transactions on Robotics and Automation, vol. 18, no. 2, pp. 121–137, 2002.

[19]. He X, Balicki M, Gehlbach P, Handa J, Taylor R, and Iordachita I, "A multi-function force sensing instrument for variable admittance robot control in retinal microsurgery," in Robotics and Automation (ICRA), 2014 IEEE International Conference on. IEEE, 2014, pp. 1411–1418.

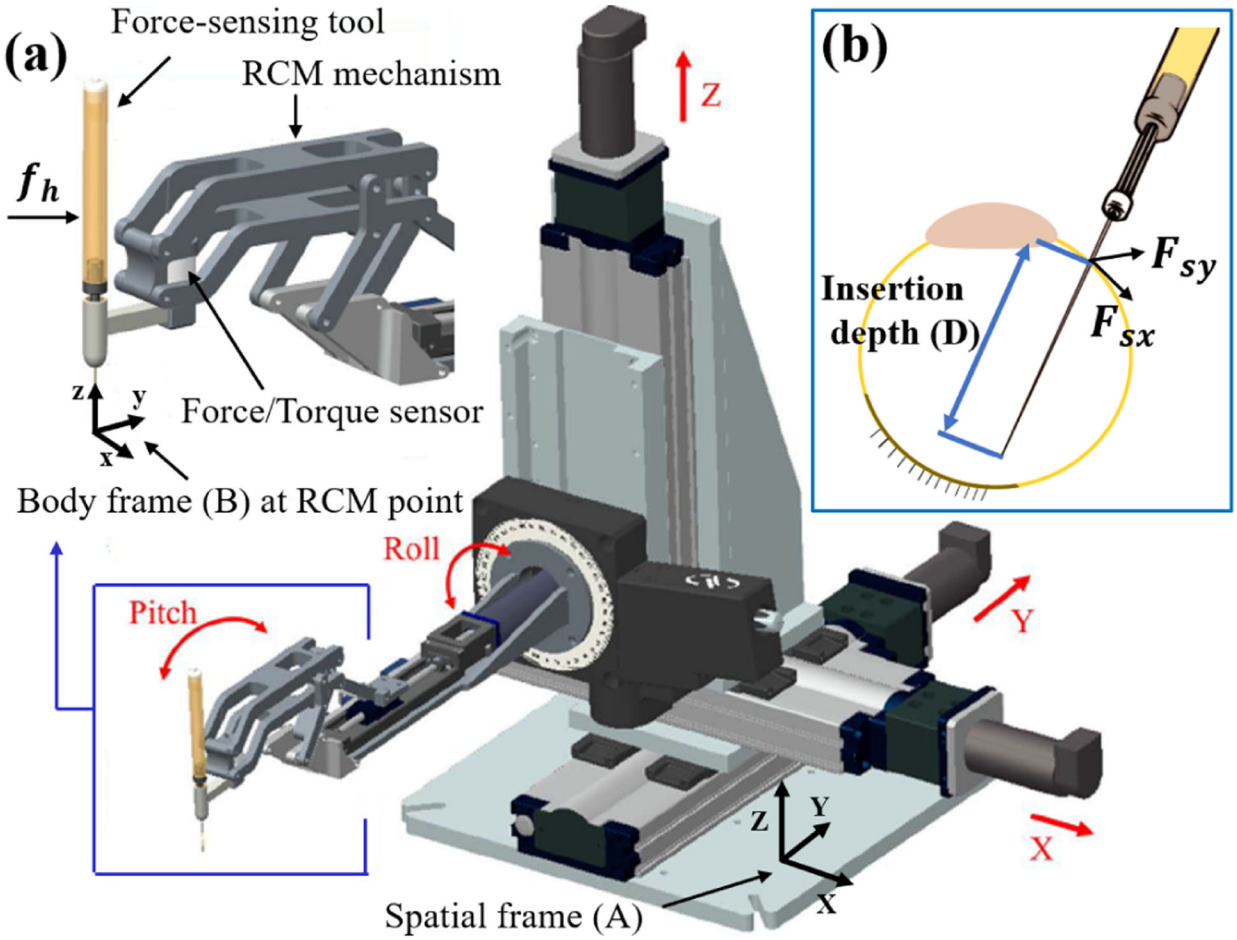

Fig. 1.

Johns Hopkins Steady-Hand Eye Robot with its five degrees of freedom shown with red marks, spatial coordinate frame at the robot base and the body coordinate frame at the RCM point (a) representation of the x and y components of the sclera force in the body frame (f_{sx} and f_{sy}) and the tool insertion depth (b)

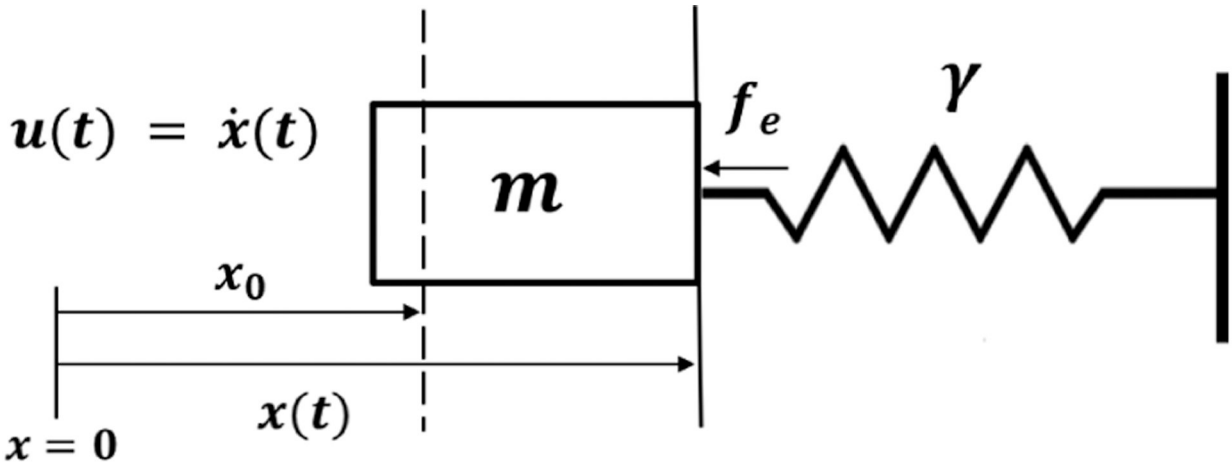

Fig. 2.

Schematic diagram for the adaptive force control of a 1-Dof velocity-controlled robot with mass m interacting with an environment with linear and unknown compliance γ.

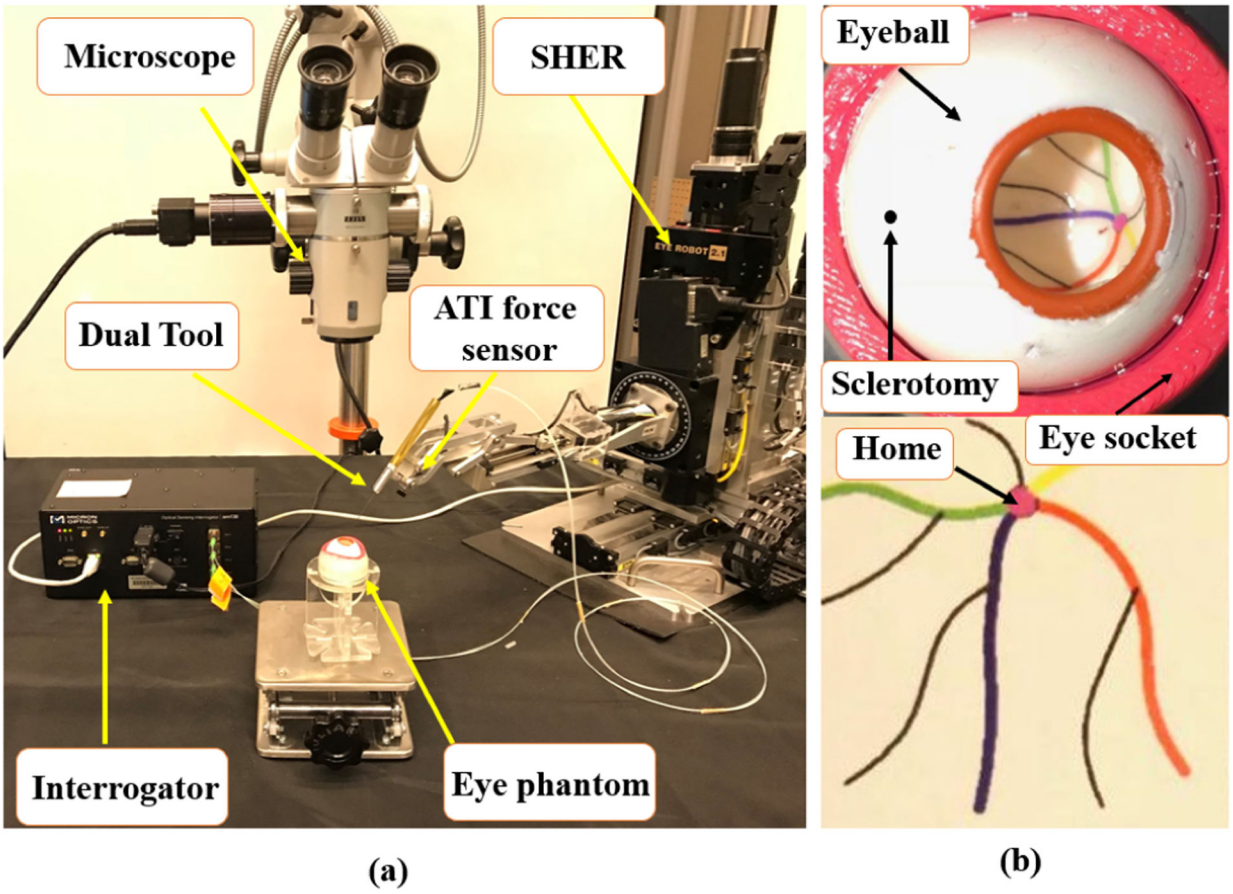

Fig. 3.

Experimental setup including the SHER, dual force-sensing tool, interrogator, microscope and eye phantom (a), Close-up view of the eye phantom and the painted vessels on the retina (b)

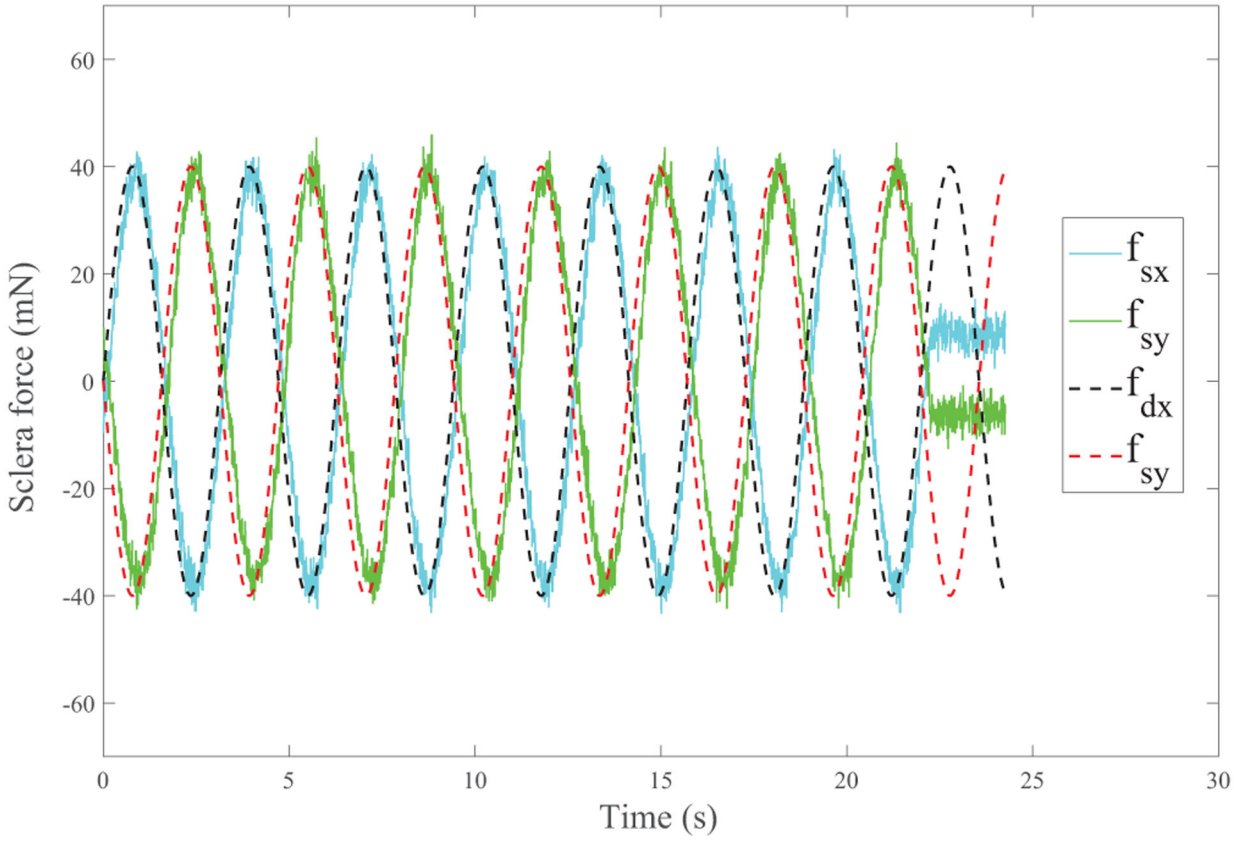

Fig. 4.

Implementation of the adaptive sclera force control for sinusoidal reference trajectories, $f_{dx} = 40sin(2t)$ mN and $f_{dy} = -40sin(2t)$ mN

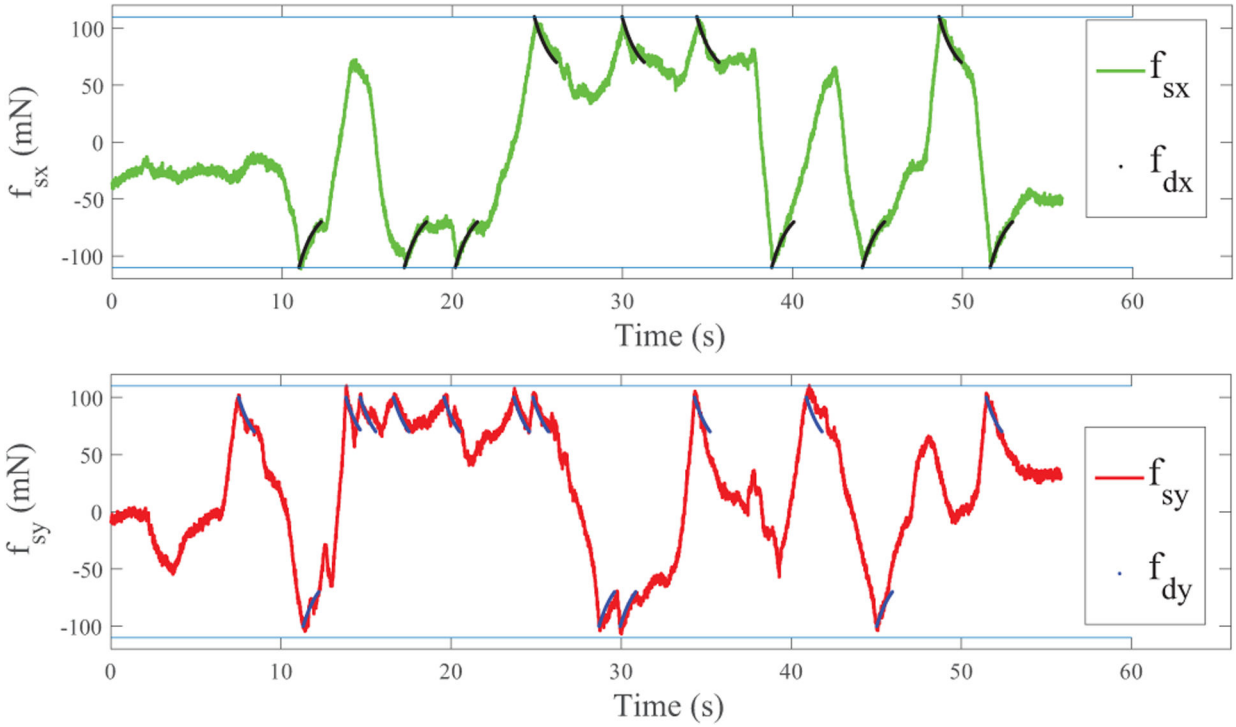

Fig. 5.

Variations of f_{sx} (top) and f_{sy} (bottom) for vessel following task, the discontinuous curves in each plot indicate the desired exponential f_{dx} and f_{dy} for the interval when the corresponding adaptive controller is activated (when $|f_{sx}|$ or $|f_{sy}|$ are between 100 and 70 mN). The horizontal lines of 120 mN and −120 mN are plotted in each figure.

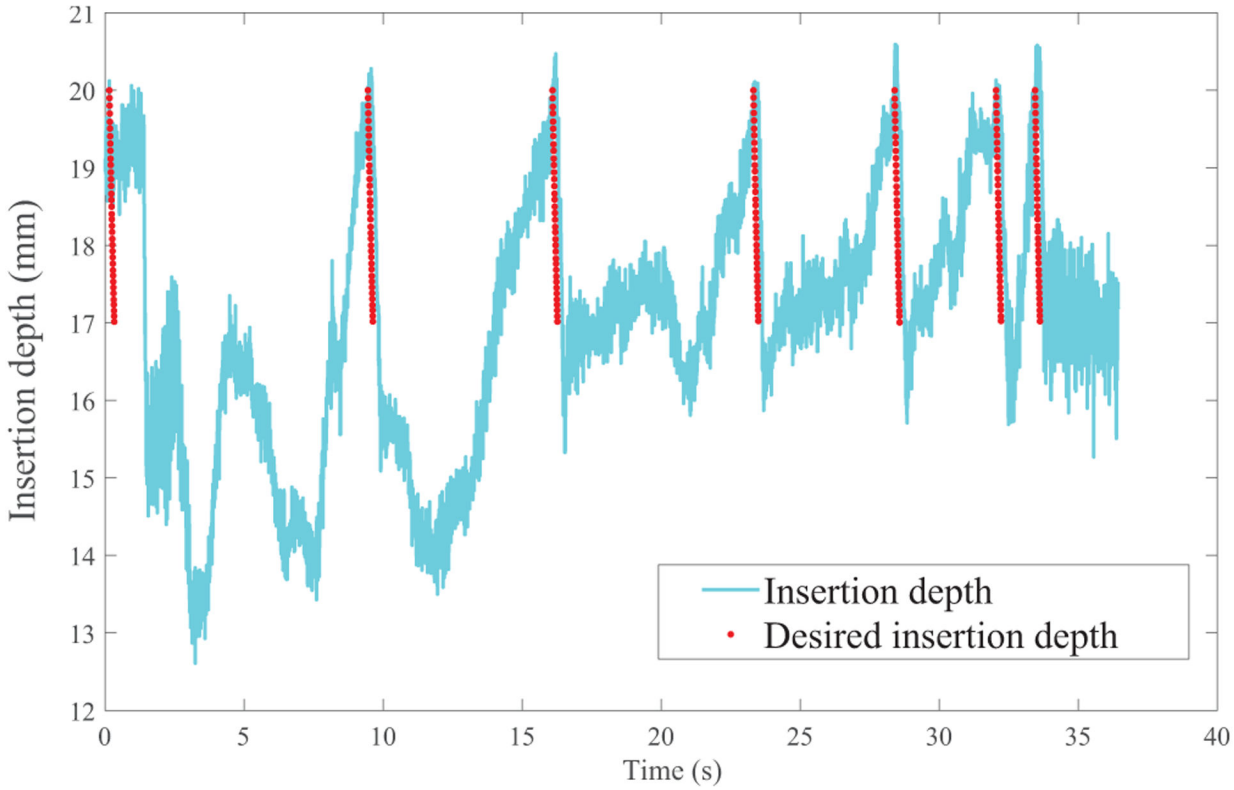

Fig. 6.

Illustration of insertion depth adaptive control when the insertion depth exceeds 20 mm. Adaptive control is active when $17 < D < 20$ mm.

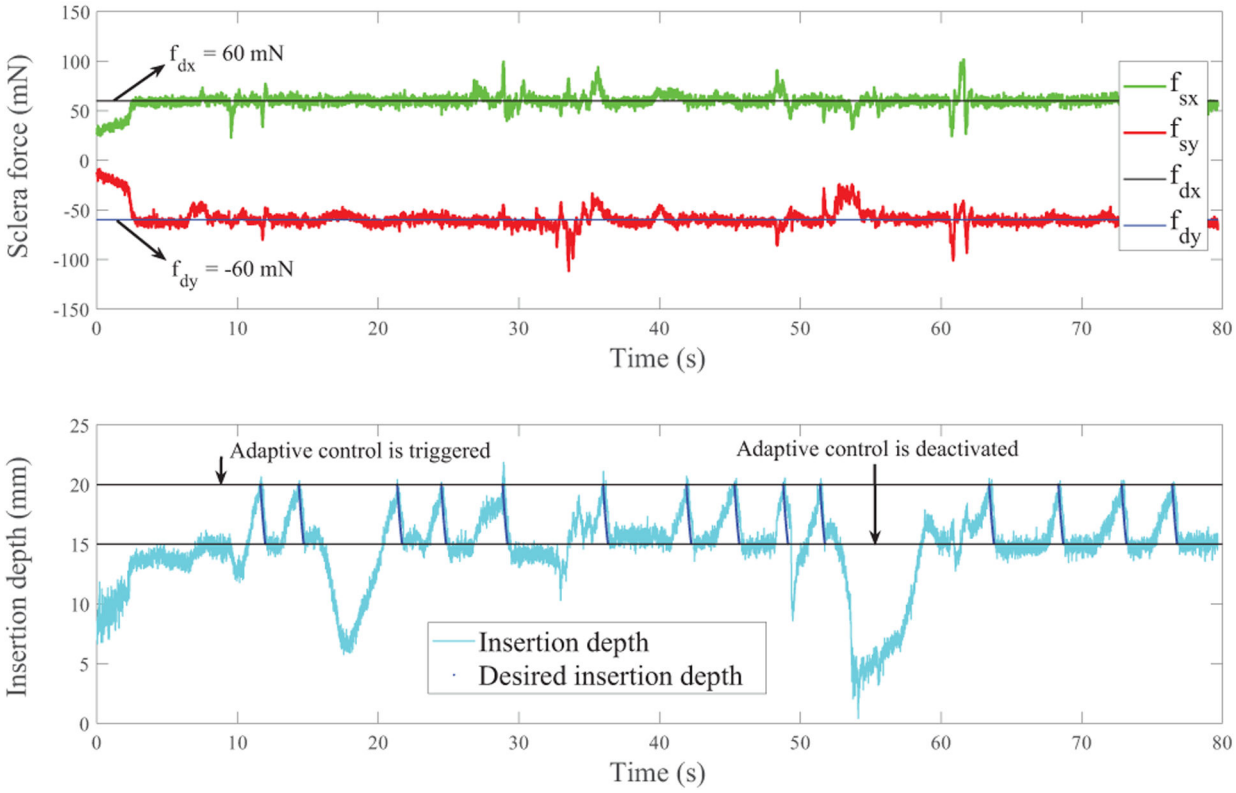

Fig. 7.

Robot-assisted light pipe holding - plots for sclera force components (top) with fixed desired trajectories and insertion depth (bottom) with exponential desired trajectory.